
Chapter 4 Low Energy Prompt Radiation Phenomena

In this chapter two special considerations pertinent to nearly all accelerators are discussed that are largely low-energy phenomena. The general behavior of both of these phenomena are nearly independent of incident particle type and energy.

I. Introduction

Accelerators of sufficient energy to produce neutrons copiously (either ion or electron accelerators) exhibit two phenomena involving low energy neutrons which must be addressed. These are the transmission of neutrons by penetrations and the control/prevention of "skyshine". For both, the neutrons involved are generally of low energy (compared to the beam particles) and the phenomena are also rather independent of the beam particle energy.

All accelerators evidence the need to control the transmission of neutrons by penetrations since all accelerators have access-ways to permit entry of personnel and equipment as well as penetrations for cables and for radio-frequency (RF) waveguides. For skyshine, while it is usually "preventable" through the application of sufficient roof shielding, all major accelerators constructed to date have encountered this problem. This has resulted either from lack of consideration of it at the design stage or from the need to accommodate other constraints such as the need to minimize the weight of shielding borne by the roofs of large experimental halls.

II. Transmission of photons and neutrons by penetrations

Personnel access penetrations will typically have cross-sectional dimensions of 1 meter by 2 meters (door-sized) while utility ducts will generally be much smaller, typically no larger than 0.2 by 0.2 m. Often the utility penetrations are partially filled with cables and other items, and even cooling water in pipes.

Two general rules are advised for such penetrations:

Penetrations should not be arranged so that a particle or photon beam is aimed directly toward it. Therefore, they should nearly always be primarily transporting *scattered* radiation through the penetrations.

The sum of the wall thickness between the source and the "outside" should be equivalent to that which would be required if the labyrinth were not present.

Before describing the details of penetration design as such, one should review some simple parameterizations of the reflections of photons and neutrons. Reflections of photons and neutrons can be treated through the use of **albedo** parameters. These have applications more general than merely the design of penetrations. They represent the ability of solid materials to "reflect" particles. Figures 4.1 and 4.2 give the albedo

Chapter 4 Low Energy Prompt Radiation Phenomena

parameters α_x and α_n for monoenergetic photons and neutrons, respectively, incident on flat surfaces of infinite dimensions of concrete plotted as functions of energy for various conditions of incidence. As is obvious from these curves, the albedo of neutrons is typically larger and somewhat less strongly dependent on energy than is that of photons. Chilton et al. has given more detailed results for concrete and for other materials (Ch63, Ch64, Ch65a, and Ch65b).

Photons

A particular application of these coefficients to the design of labyrinths is given here to illustrate usage of such albedo curves. Figure 4.3 shows an example of a labyrinth providing access to a collimated photon source of some known dose equivalent (or dose equivalent rate), H_0 , at one meter. In general, some knowledge of the photon energy spectrum at this location is also needed. Such a photon "beam" is relevant to the subject of this text because, for example, it could arise from the targetry of a beam from an electron accelerator. With the reflection coefficients α_x , one can use the following formula to obtain a conservative estimate of the dose equivalent (or dose equivalent rate), H_{rj} , after j sections (not counting the initial path length to the wall, d_i) of the maze:

$$H_{rj} = \frac{H_0 \alpha_i A_i \prod_{k=1}^j \alpha_k A_k}{d_i^2 \prod_{k=1}^j d_{rk}^2} \quad j \geq 1. \quad (4.1)$$

In this formula, the coefficient α_i is selected to be representative of the initial photon energy while A_i estimates the cross sectional area of the wall struck by the initial photons evaluated by projecting the beam cross-sectional area to the wall. For successive legs after the first, taking the value of α appropriate for 0.5 MeV photons is often considered to be a conservative approach. This is substantiated physically because if E_0 is the initial photon energy in MeV, the photon energy, E_{scatt} (MeV), following Compton scattering is given by:

$$E_{scatt} = \frac{E_0}{1 + (E_0 / 0.511)(1 - \cos\theta)}. \quad (4.2)$$

Thus, E_{scatt} has a maximum value of 0.511 MeV after a scatter of 90° for $E_0 \gg 0.511$ MeV.

A_k is the cross-sectional area of the k^{th} leg of the maze. If the maze is uniform with cross section A , and has j legs, then the product in the numerator is simply raised to the j^{th} power; $(\alpha A)^j$. In the denominator, the distances are just those defined in Fig. 4.3 and, of course, represent the inverse-square law dependence. This formula is more conservative for photon energies exceeding 10 MeV, but at the higher energies the uncertainties are larger. The above formula is probably most accurate if the ratios $d_{rk}/(A_k)^{1/2}$ lie between 2 and 6.

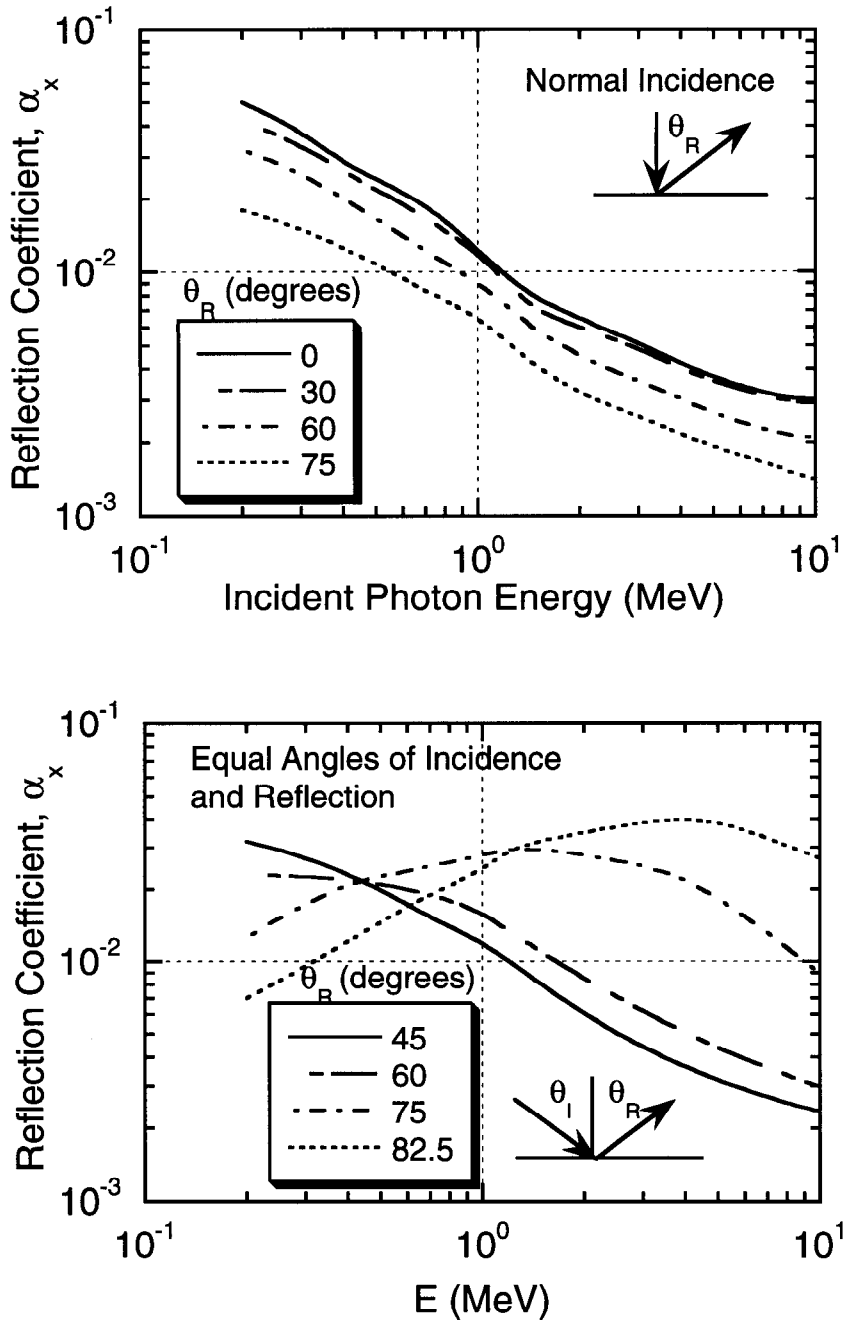


Fig. 4.1 Reflection coefficients, α_x , for monoenergetic photons incident on ordinary concrete as a function of incident photon energy, for several angles of reflection assuming normal incidence and for equal angles of incidence and reflection. For photon energies higher than 10 MeV, the use of the 10 MeV values of α_x is expected to be conservative. [Adapted from (NC77) and references cited therein.]

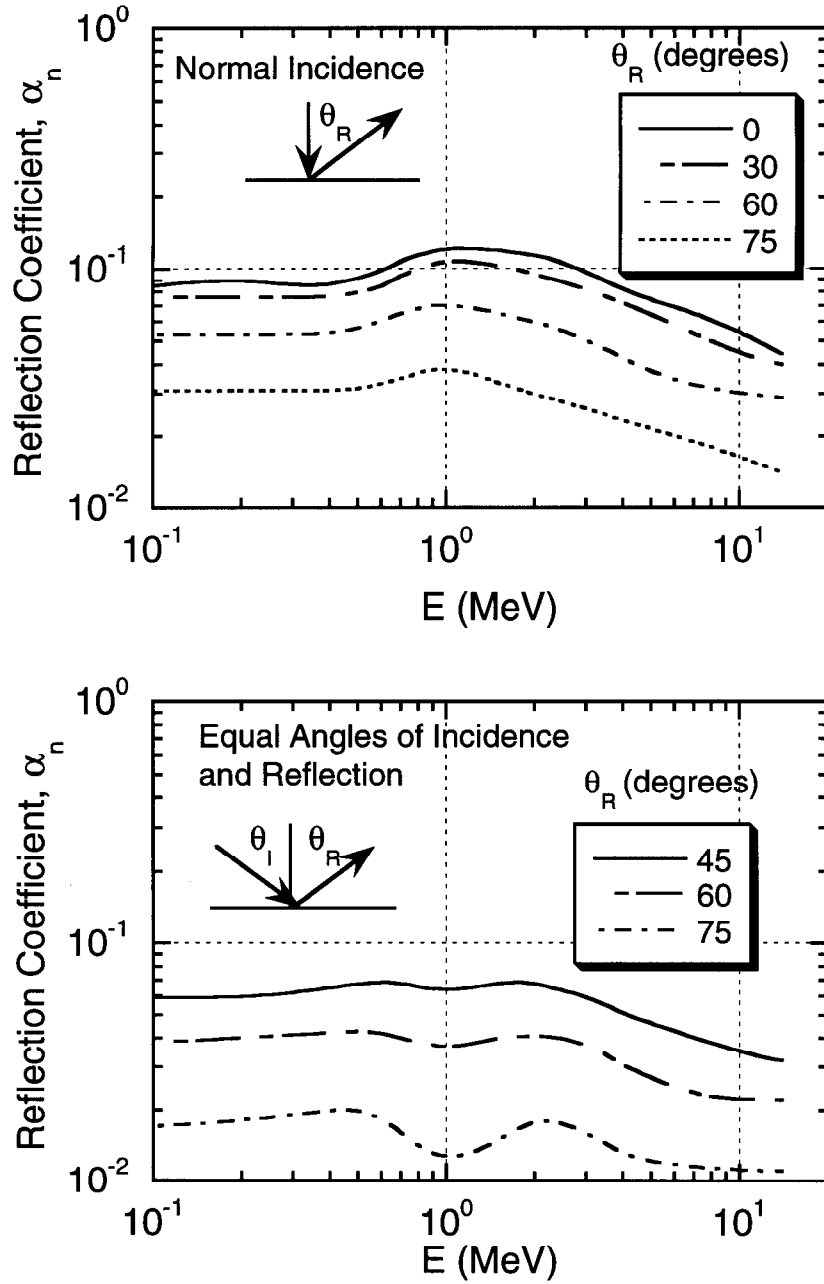


Fig. 4.2 Reflection coefficients, α_n , for monoenergetic neutrons incident on ordinary concrete as a function of incident neutron energy, for several angles of reflection assuming normal incidence and for equal angles of incidence and reflection. [Adapted from (NC77) and references cited therein.]

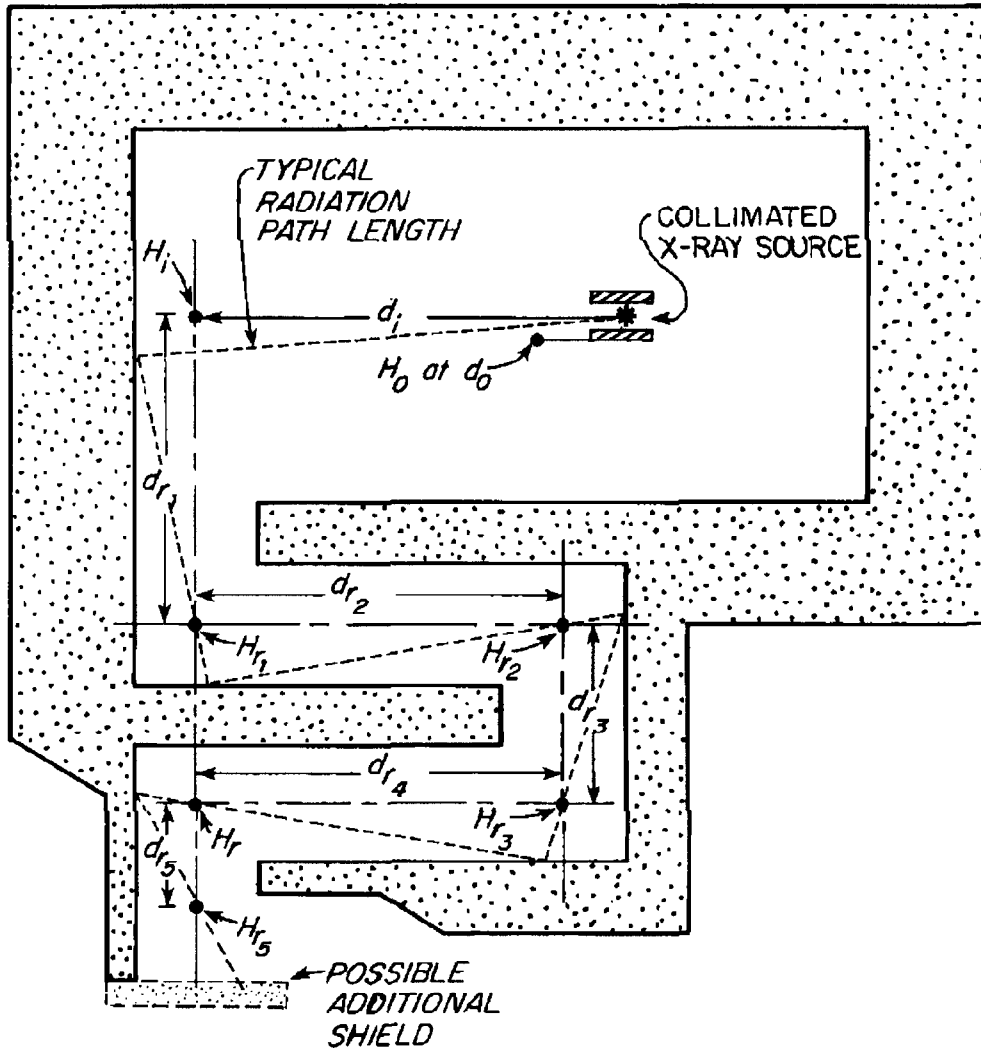


Fig. 4.3 Generalized labyrinth design illustrating successive reflections of photons from a collimated source through the maze. The source could just as well originate from an electron beam originating from the right side of the figure incident on a target located at the point in space labeled "collimated x-ray source". The various path lengths can be approximated by a sequence of centerline distances, as shown in the diagram. [Reproduced from (NC77).]

Neutrons

Unfortunately, complications in the transport of neutrons discourage the use of a similar formula. The radiation source, or potential radiation source for situations of concern from the standpoint of accidental beam losses, should be evaluated according to the methods described previously. Typical methods for addressing the attenuation of radiation by penetrations involve the use of the results of calculations made by sophisticated Monte-Carlo codes. These can be used for both curved and rectilinear labyrinths with the primary practical experience being with the latter type. In this section, the results of such work will be presented in order to give the reader useful information in the evaluation of such penetrations. A typical rectilinear personnel access labyrinth is shown in Fig. 4.4.

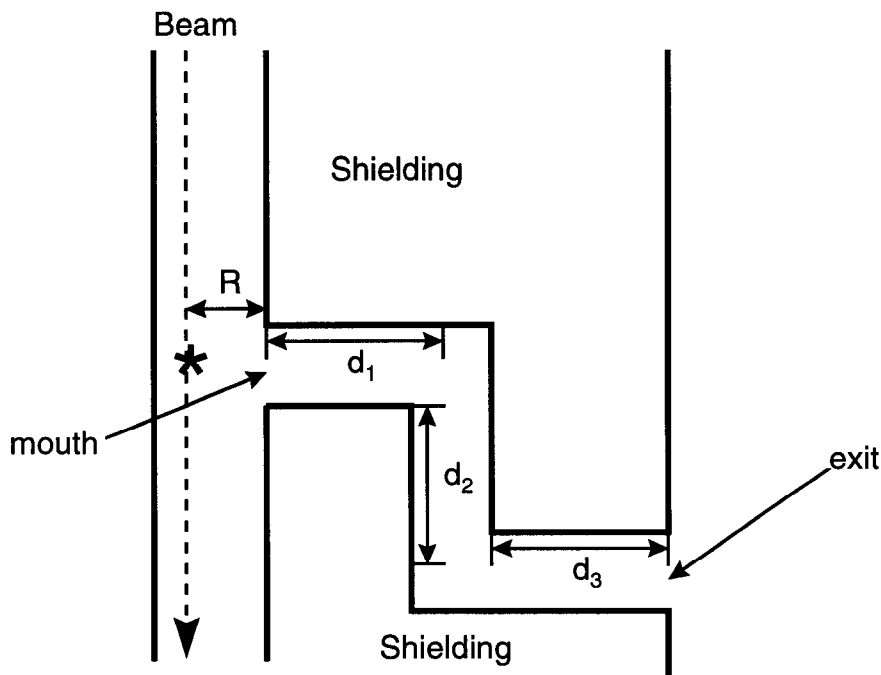


Fig. 4.4 Schematic plan view of a typical personnel access labyrinth of three "legs" at a large accelerator facility which defines the coordinate system and terminology associated with labyrinth calculations. The (*) denotes the location of a loss of beam at a point adjacent to the "mouth" of the labyrinth.

An overwhelming conclusion drawn from existing data is that the bombarding particle energy has very little effect upon the attenuation of a labyrinth viewing a source of beam loss other than the fact that the total yield of "source" neutrons increases as a function of incident energy and ion type. One can thus estimate the dose, dose equivalent, or neutron fluence at the exit of a labyrinth by using attenuation estimates in conjunction with an estimate of the neutron fluence or dose equivalent found at the entrance of the penetration into the beam enclosure. This "factorization" approximation allows attenuation measurements and calculations obtained at proton accelerators to be of rather general utility.

Chapter 4 Low Energy Prompt Radiation Phenomena

For penetrations exposed to targets struck by hadrons, we first consider the straight penetration studied by Gilbert et al. (Gi69) which measured the transmission of an exceptionally long straight tunnel of dimensions 2.8 m high by 1.8 m wide and 100 m long. 14 GeV protons were incident on a target providing a good "point source" 3.2 m from the tunnel mouth. The use of a set of activation detectors having different energy thresholds made it possible to obtain some information about the neutron energy spectrum. The measurement technique employed will be reviewed in somewhat more detail in Chapter 5. The experimental conditions did not allow an absolute normalization to beam loss. Table 4.1 gives the thresholds or approximate sensitive ranges of various nuclear reactions used in this particular measurement. The dosimeters used to detect photons are also sensitive to gamma rays produced by the capture of neutrons by the nuclei in the air and in the tunnel walls. The results of the measurements are presented in Fig. 4.5. The "fits" shown in this figure were arbitrarily normalized to the measurements at a depth of 20 meters in the tunnel and assumed an exponential attenuation multiplied by an inverse square-law dependence. It is clear that neutrons of lower energy attenuate more rapidly by air and wall-scattering than do the higher energy neutrons. For short tunnels (< 20 m long) the "attenuation" of the fast neutrons is almost entirely accomplished by inverse-square law considerations. Accounting for the inverse-square dependence for this long tunnel, the attenuation is well-described by exponential absorption functions having effective mean free paths, $\lambda(E)$, corresponding to energy-dependent removal cross sections. The $\lambda(E)$ values are given in Table 4.2. The effective removal cross sections determined by this measurement are about a factor of 1.5 to 2 smaller than those that would be inferred from the known absorption cross sections of the constituents of air. This may well be evidence of "in-scattering" by the concrete walls since more neutrons than expected were observed at the larger distances into the tunnel.

Table 4.1 Detectors and their characteristics as used in the measurements summarized in Fig. 4.5. The sensitive energy ranges are approximate.

Detector	Nuclear Reaction	Energy Range (MeV)
$\beta\gamma$ Dosimeters	photons and charged particles	all
Gold (Au)	$^{197}\text{Au}(n,\gamma)^{198}\text{Au}$	Thermal Energies
Aluminum (Al)	$^{27}\text{Al}(n,\alpha)^{24}\text{Na}$	$E > 6$ MeV
Carbon (C)	$^{12}\text{C}(n,2n)^{11}\text{C}$	$E > 20$ MeV

Table 4.2 Mean free paths and removal cross sections for tunnel transmission as exhibited by the measurements summarized in Fig. 4.5. [Adapted from (Gi69).]

Detector	Mean Free Path (meters)	Inferred Removal Cross Section (barns)
$\beta\gamma$ Dosimeters	55	3.3
Gold (Au)	30	6.2
Aluminum (Al)	60	3.2
Carbon (C)	100	1.9

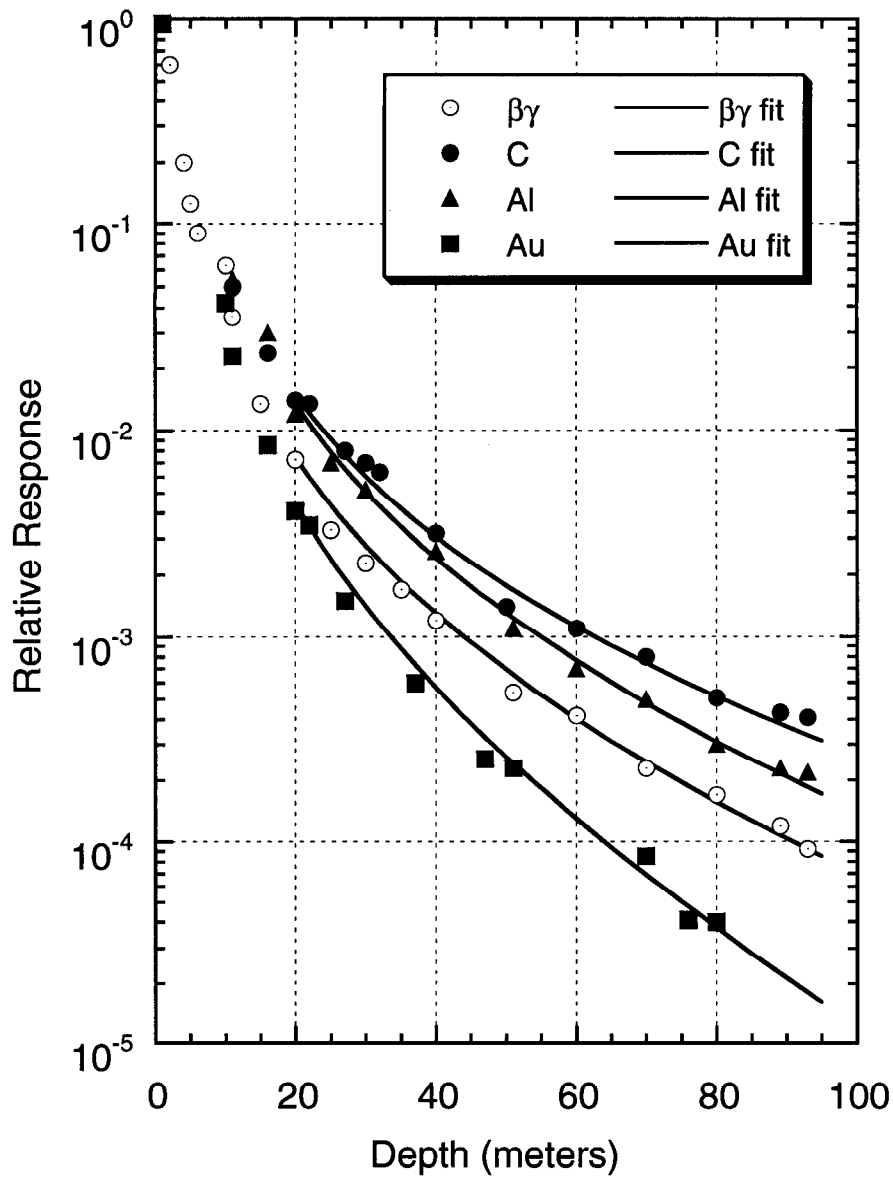


Fig. 4.5 The relative transmission of neutron flux density and gamma dose rate along a large straight tunnel described in the text. The measurement results are shown as the symbols while the solid lines represent the fits described in the text arbitrarily normalized at a depth of 20 meters. [Adapted from (Gi69).]

An important "rule of thumb" is that the attenuation of neutrons in labyrinths generally scale with a unit length equal to the square root of its cross-sectional area provided that the height to width ratio does not vary greatly outside of the range 0.5 to 2.0 (Th88). Of course, details of the source geometry are very important in such a straight penetration.

Chapter 4 Low Energy Prompt Radiation Phenomena

Goebel [(Go75) and summarized in (Sc90)] has calculated universal attenuation curves for "first" legs of labyrinths (i.e., those sections first encountered as one moves outward from the beam). Goebel used and compared results from the codes SAM-CE (Co73), AMC (Ma67), and ZEUS (D'H68). Gollon and Awschalom (Go71) have generated similar curves using the ZEUS code for a variety of geometries. The three situations of point source, line source, and plane or point source off axis for a straight tunnel displayed as universal dose attenuation curves as calculated by Goebel are given in Fig. 4.6. An "off axis point source" is one that is not centered in front of the labyrinth mouth. The distance down the passageway, as is customary, is expressed in units of the square root of the cross-sectional area of the passageway. It is obvious that extended, or "off axis", sources are more readily attenuated because the tunnel aperture provides less "acceptance".

It has been found by Cossairt (Co95) that the point source dependence calculated by Goebel can be approximated by the following expression:

$$H_1(d_1) = \left[\frac{r_o}{d_1 + r_o} \right]^2 H_o(R) \quad (4.3)$$

where r_o is simply a fitting parameter that has the value of

$$r_o = 1.4, \quad (4.4)$$

$H_1(d_1)$ is the dose equivalent distance d_1 in the first leg as measured from the mouth of the passageway in "units" of the square root of the cross-sectional area of the first leg. $H_o(R)$ is the dose equivalent at the mouth the determination of which will be discussed later. The result of this fit is displayed in Fig. 4.6. Over the domain of $0 < d_1 < 9$ the expression fits the Goebel curve within ± 10 per cent, certainly sufficiently accurate for radiation protection purposes. The domain of d_1 is the appropriate one given the fact that most "personnel" labyrinths are of cross-sectional area of about $1 \times 2 \text{ m}^2$. Hence, the unit length is approximately 1.4 meters. A 10 "unit" long first leg is, typically, about 14 meters (or about 46 feet) which is quite long compared with typical labyrinth legs.

Tesch (Te82) has developed a very simple approach to the problem of dose equivalent rate attenuation by multi-legged labyrinths at proton accelerators that are typical of personnel accessways of approximately 2 m^2 cross section. For the first leg the expression is an inverse-square law dependence with a simple "in-scattering" factor of two included,

$$H_1(d_1) = 2H_o(R) \left(\frac{R}{d_1} \right)^2. \quad (4.5)$$

This formula does not scale the distances by the cross-sectional area of the passageway and, presumably, is valid only for personnel passageways of approximately 2 m^2 cross section.

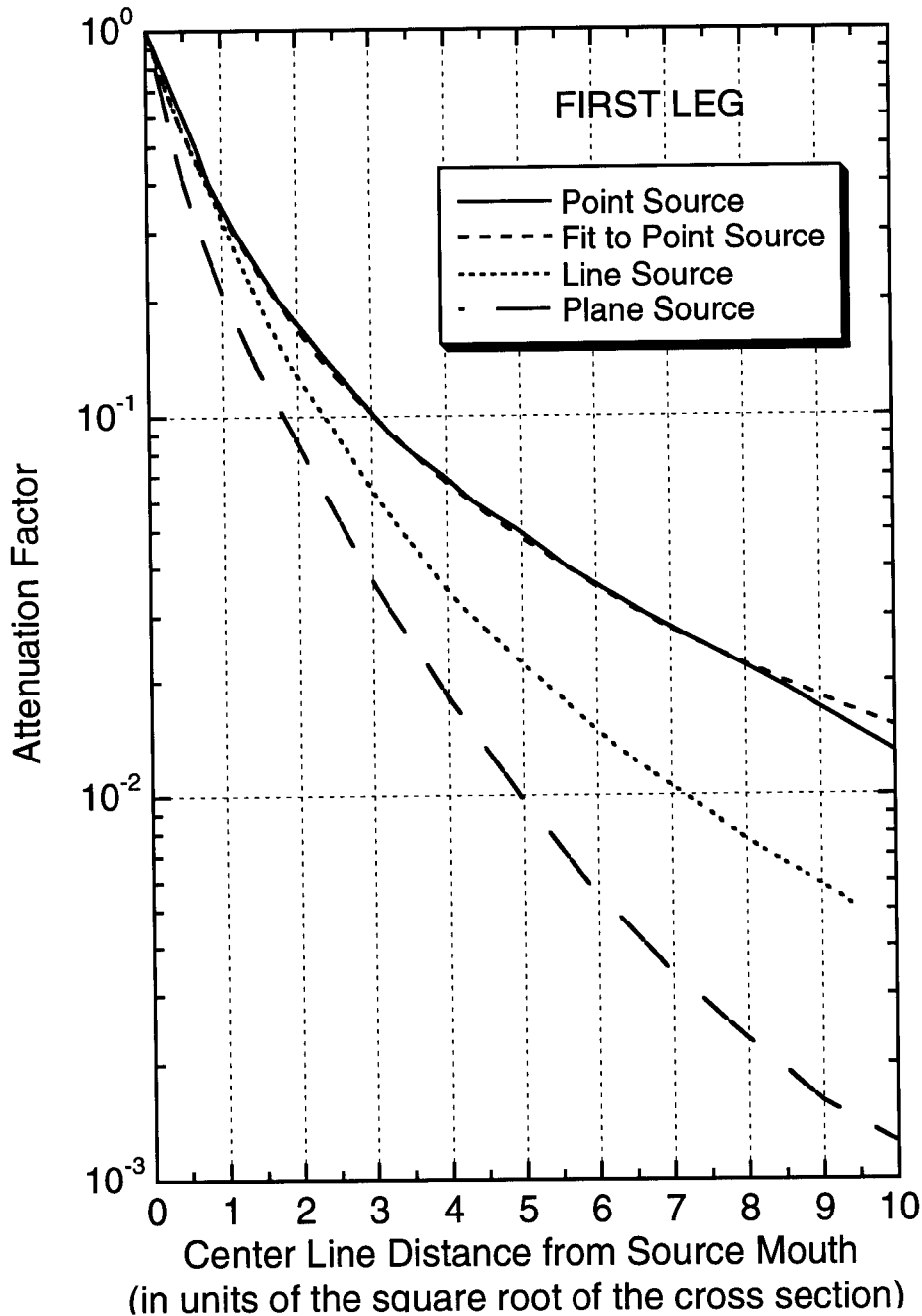


Fig. 4.6 Universal transmission curves for the first leg of a labyrinth. The fit for the point source curve represented by Eq. (4.3) is also included. The curve for a plane source is also suitable to use with an off axis point source. [Adapted from (Go75) and (Co95).]

Chapter 4 Low Energy Prompt Radiation Phenomena

Stevenson and Squier reported the results of measurements in a two-legged penetration at the NIMROD synchrotron (St73). This penetration was of cross section $2.3 \times 2.3 \text{ m}^2$ and the walls were made of concrete. The target at the mouth of the labyrinth was bombarded by 7 GeV protons. Figure 4.7 is a plot of the transmission of particle flux density along this tunnel using different nuclear reactions, again used because of their thresholds. One can see that, proceeding from the target outward in the passageway, beyond the abrupt jump which arises as the corner hides the target from view, the fast neutron components are attenuated more readily than is the thermal one. This phenomena associated with "turning the corner", was also verified by Cossairt et al. (Co85a).

Second and successive legs of such "rectilinear" penetrations thus change the situation dramatically, principally by modifying the spectrum of the transmitted neutrons. Fig. 4.8 is a universal curve for second and succeeding legs which is a companion to that given for the first leg in Fig. 4.6. It was found by Cossairt (Co95) that the following expression adequately describes this curve,

$$H_i(d_i) = \left\{ \frac{\exp(-d_i / a) + A \exp(-d_i / b) + B \exp(-d_i / c)}{1 + A + B} \right\} H_{i-1}(d_{i-1}) \quad i^{\text{th}} \text{ leg } (i > 1), \quad (4.6)$$

where the fitting parameters are:

$$\begin{aligned} a &= 0.17 \\ b &= 1.17 \\ c &= 5.25 \\ A &= 0.21 \\ B &= 0.00147. \end{aligned}$$

The results of this fit are also included in Fig. 4.8.

Tesch (Te82) also has developed a formula for the transmission of the second and successive legs which is,

$$H_i(d_i) = \left\{ \frac{\exp(-d_i / 0.45) + 0.022 A_i^{1.3} \exp(-d_i / 2.35)}{1 + 0.022 A_i^{1.3}} \right\} H_{i-1} \quad (i^{\text{th}} \text{ leg}, i > 1) \quad (4.7)$$

Here, A_i is the cross sectional area of the i^{th} leg in units of square meters. As was the case with respect to Eq. (4.5), this formula uses the distances, d_i (meters), along the labyrinth directly and does not scale them against the square root of the cross sectional area. Again, it is valid for "door-sized" labyrinths having cross sectional areas of approximately 2 m^2 .

In Fig. 3.22 is shown a four-legged labyrinth providing entrance to a tunnel above a target stuck by 400 GeV protons accelerated by the Tevatron at Fermilab. Figure 4.9 compares experimental measurements (Co85a) of absorbed dose throughout this labyrinth with several methods of calculation. As one can see, all methods of calculating the attenuation are approximately valid even for this four-legged labyrinth. The assumption that

Chapter 4 Low Energy Prompt Radiation Phenomena

succeeding legs can be considered the same as the second leg is thus approximately verified.

For this labyrinth, a recombination chamber technique (see Chapter 6) was used to measure the neutron quality factor, Q , at two locations, one at the end of the first leg and one in the middle of the short second leg. These locations are denoted R in Fig. 3.22. The results were $Q = 5.5 \pm 0.6$ and $Q = 3.4 \pm 0.1$, respectively. This indicates a softening of the neutron energy spectrum in the second leg which was further verified by a measurement of the neutron energy spectrum using a multisphere technique (see Chapter 6) which resulted in $Q = 3.1 \pm 0.7$. This spectrum, measured at the location denoted S , is also shown in Fig. 3.22. The measured second-leg spectrum exhibited domination by thermal, or near-thermal neutrons. It is clear that several approaches to the design of labyrinths are equally effective for practical radiation protection work.

Curved tunnels are principally used to provide access for large equipment items that cannot negotiate right-angle bends. These have not been treated in nearly the same detail as have the rectilinear passageways. It appears that the attenuation is effectively an exponential with an attenuation length, λ , a function of only the radius R of the tunnel. Patterson and Thomas (Pa73) determined that

$$\lambda = 0.7\sqrt{R}, \quad (4.8)$$

where R is in meters and $4 < R < 40$ meters .

A final piece of information that is needed in practical labyrinth calculations is the answer to the following question: "What happens to the neutrons beyond the "exit" to the passageway?"

Direct observational evidence is that beyond the exit, the neutrons "disappear" rather rapidly. This phenomenon is probably due to the fact that the neutron energy spectrum is heavily dominated by thermal and near-thermal neutrons in all "legs" after the first. Such neutrons, therefore, having suffered many scatters would not be collimated in any particular direction. Elwyn (El91) has quantified this phenomenon by assuming that the exit of the labyrinth is a circular disk of area A (equivalent in area to that of the exit opening). Further, it is assumed that the neutrons emerge from this disk at all random directions with source strength (neutrons/unit area, during some time interval) S_A . Fig. 4.10 illustrates the geometry. Further, it is assumed that there is only emission into the 2π steradian hemisphere outside the exit. Then the differential flux density at P on the axis of the disk is:

$$d\phi = \frac{S_A \cos \alpha dA}{2\pi\rho^2} \quad (4.9)$$

where $dA = r dr d\theta$, $\rho^2 = h^2 + r^2$, and angle α is defined in Fig. 4.10 ($\cos \alpha = h/\rho$). The $\cos \alpha$ factor is present to take into account the area of the source elemental area projected in the direction of point P . Thus,

$$d\phi = \frac{S_A h R dr d\theta}{2\pi \rho^3}. \quad (4.10)$$

Integrating,

$$\begin{aligned} \phi(h) &= \frac{S_A h}{2\pi} \int_0^R dr \int_0^{2\pi} d\theta \frac{r}{(r^2 + h^2)^{3/2}} = S_A h \int_0^R dr \frac{r}{(r^2 + h^2)^{3/2}} = \\ &= S_A h \left[\frac{-1}{\sqrt{r^2 + h^2}} \right]_0^R = S_A \left[1 - \frac{1}{\sqrt{1 + \left(\frac{R}{h}\right)^2}} \right], \end{aligned} \quad (4.11)$$

where attenuation by the air is neglected. Thus one can use this by approximating the area of the exit opening by the area of a disk have an equivalent area. The rapidity of the decrease of fluence is illustrated by the tabulation of a few values in Table 4.3.

At large distances, one can apply a "point source" approximation due to the fact that:

$$\phi(h) \approx \frac{S_A}{2} \left(\frac{R}{h}\right)^2 \quad \text{for } h \gg R. \quad (4.12)$$

For $h = 0$, $\phi(0) = S_A$ as expected.

To summarize so far; one can use a calculation or measurement of the neutron flux density or dose equivalent at mouth of the labyrinth in conjunction with one of the above methods of calculating the attenuation of the neutrons by the passageway to get an estimate of the dose equivalent or fluence at the exit of the passageway.

Generally, the dose at the entrance can be obtained using Monte-Carlo techniques or by directly using the information about neutron yields. Approximations that use Moyer Model parameters discussed in Chapter 3 are likely to overestimate the dose equivalent at the entrance. This is due to the fact that the Moyer parameter implicitly assumes development of the shower (a "buildup" mechanism, as seen in Chapter 3) in the enclosure shielding which is, in effect, short-circuited by the passageway.

For high energy proton accelerators, a rule of thumb for the source term which has been found to be very successful for the degree of accuracy generally required for personnel protection purposes has been developed by Ruffin and Moore (Ru76). It was improved by inclusion of the Moyer energy scaling by Rameika (Ra91). In this model, it is seen that about one fast neutron/GeV of proton beam energy is produced with an isotropic distribution in addition to the much higher multiplicity in the forward direction. The neutrons that will dominate the spectrum and determine the dose equivalent at the entrance to the labyrinth have kinetic energies between 1 to 10 MeV. From the dose equivalent/fluence factors, $P(E)$, in Fig. 1.5, 1 rem of 10 MeV neutrons represents a fluence of approximately $3 \times 10^7 \text{ cm}^{-2}$ for neutrons over this energy domain.

Chapter 4 Low Energy Prompt Radiation Phenomena

Thus, at distance R (cm) from the source, one obtains;

$$H(\text{rem}) = \frac{E_0^{0.8} N_p}{4\pi R^2 (3 \times 10^7)} = 2.65 \times 10^{-9} \frac{E_0^{0.8} N_p}{R^2}. \quad (4.13)$$

where R is in cm, E_0 is in GeV, and N_p is the number of incident protons. The constant, 2.65×10^{-9} (rem cm²), turns out to be approximately 1/3 the value obtained by using the Moyer source (see Chapter 3) parameter along with the Moyer angular factor at $\theta = \pi/2$;

$$(2.8 \times 10^{-7} \text{ rem cm}^2) \exp(-2.3\pi/2) = 7.6 \times 10^{-9} \text{ rem cm}^2. \quad (4.14)$$

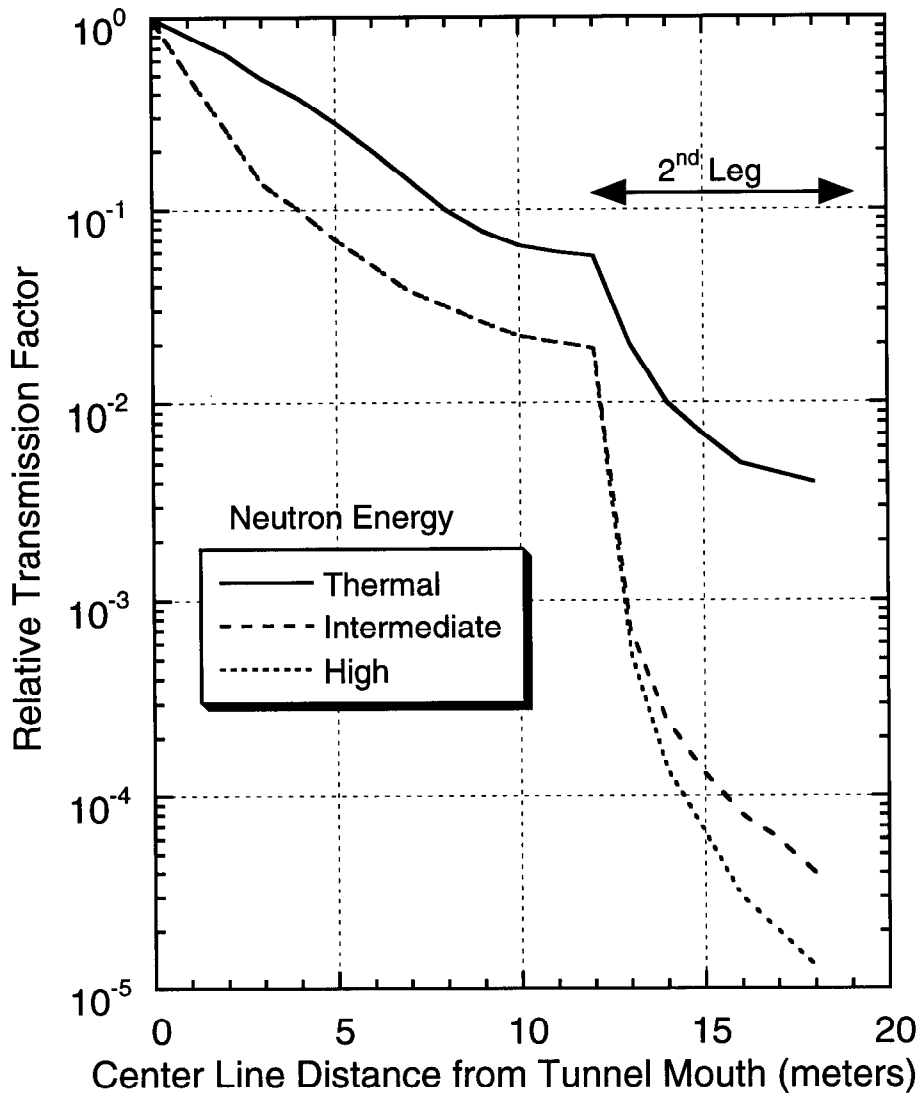


Fig. 4.7 Relative transmission of particle flux density along a two-legged labyrinth using threshold detectors. The curve labeled "intermediate" corresponds to neutrons having energies between approximately 6 and 25 MeV while the curve labeled "high" corresponds to neutron energies above 20 MeV. [Adapted from (St73).]

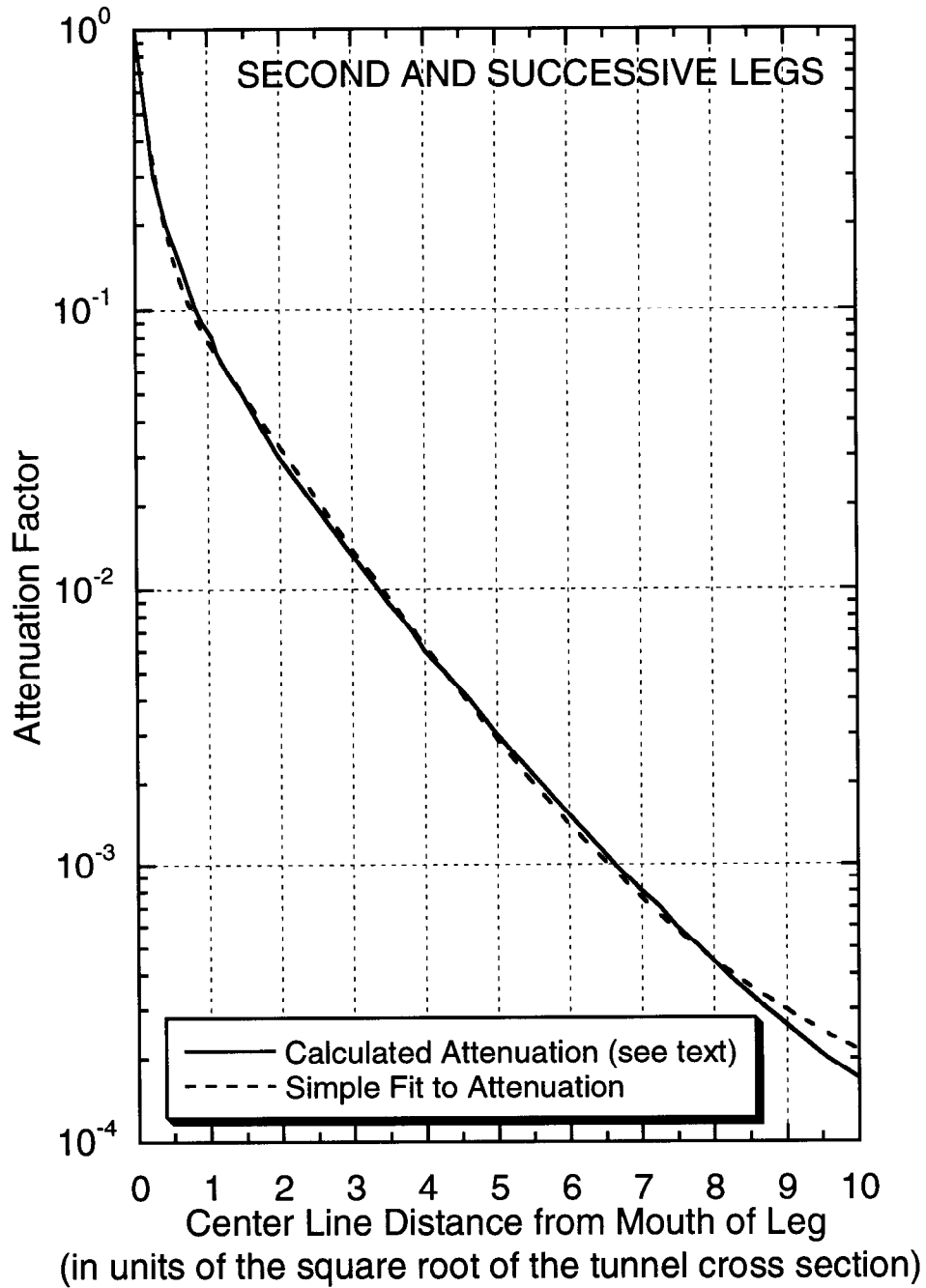


Fig. 4.8 Universal transmission curve for the second and subsequent legs of labyrinths. The calculated attenuation (solid curve) is the calculation made using AMC by Goebel et al. (Go75). The dashed curve is the fit provided by Eq. (4.6). [Adapted from (Go75) and (Co95).]

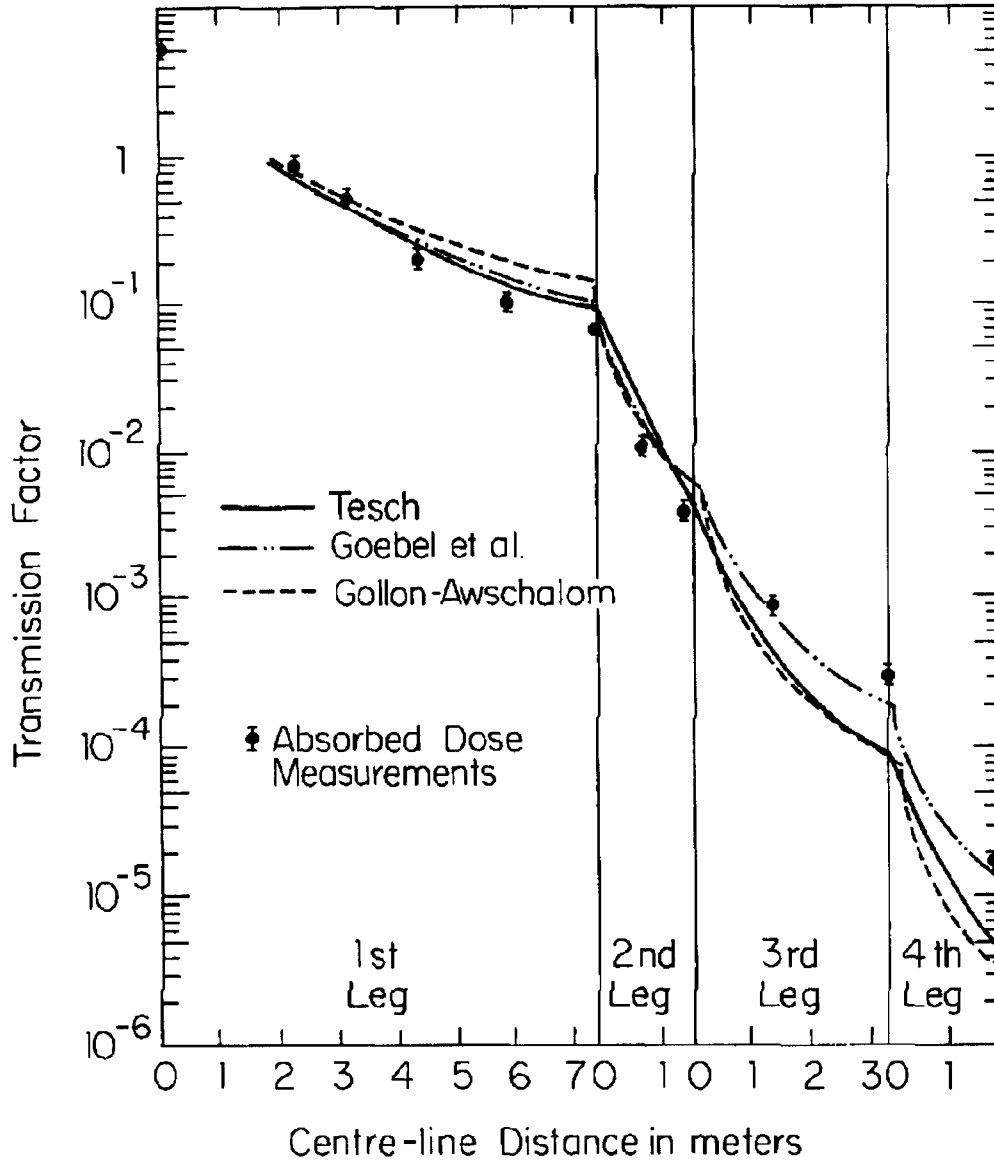


Fig. 4.9 Measurements and predictions of transmission in a tunnel at Fermilab. The results of Tesch (Te82), Goebel et al. (Go75), and Gollon and Awschalom (Go71) are compared with measurements of absorbed dose conducted at the position shown in the four-legged labyrinth displayed in Fig. 3.22. As a coincidence, the "Transmission Factor" plotted as the ordinate is also the absolute scale of the absorbed dose measurement in units of $\text{mrad}/10^{11}$ incident protons. [Reproduced from (Th88) and (Co85a).]

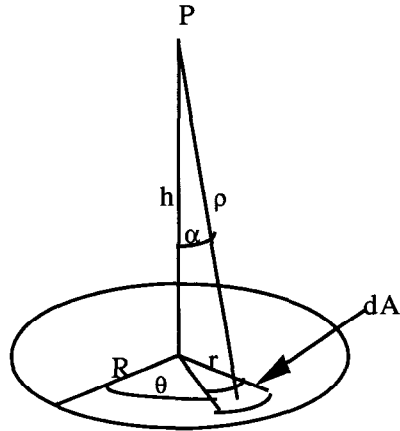


Fig. 4.10 Diagram of labyrinth exit neutron calculation. The coordinates are explained in the text.

Table 4.3 Estimates of relative neutron flux or dose equivalent as a function of scaled distance from the exit of a labyrinth.

h/R	$\phi(h)/S_A$
0.5	0.55
1.0	0.29
2.0	0.11
4.0	0.03
10.0	0.005

III. Skyshine

Thin roof shielding represents a serious problem that has plagued a number of accelerators such as the Cosmotron (BNL), the Bevatron (LBL), and the Fermilab experimental areas. The phenomenon, known as **skyshine**, is the situation in which the roof of some portion of the accelerator or an associated experimental facility is shielded more thinly than are the sides of the same enclosure that directly view the radiation source. The first attempt to calculate the skyshine radiation field was made by Lindenbaum (Li61). Schopper et al. (Sc90) gives a rather complete description of the phenomena and Patterson and Thomas (Pa73), Rindi and Thomas (Ri75), Stevenson and Thomas (St84), and Cossairt and Coulson (Co85b) present some specific results.

When addressing the skyshine question, it is generally customary to plot the neutron fluence, or even the dose equivalent, as a function of distance from the source by multiplying it by the square of the distance from the source, i.e., as $r^2 \Phi(r)$. Stevenson and Thomas (St84) included plots a number of measurements of neutron skyshine obtained at proton accelerators producing protons of energies ranging from 30 MeV to 30 GeV and also at high energy electron accelerators having energies of 7.5 and 12 GeV. In general, the quantity $r^2 \Phi(r)$ is characterized by a buildup followed by an exponential falloff. Most skyshine distributions are isotropic (i.e., independent of the angle θ). As exhibited by the typical skyshine data, λ , the effective attenuation length, has been found to vary between a minimum value of about 200 meters and much larger values which approach one kilometer. We shall shortly see how this quantity is dependent upon the energy spectrum of the neutron radiation field that is the source of the skyshine.

Patterson and Thomas (Pa73) give a formula that describes such behavior for $r > 50$ meters.

$$\Phi(r) = \frac{aQ}{4\pi r^2} (1 - e^{-r/\mu}) e^{-r/\lambda} \quad (4.15)$$

In this equation, $a = 2.8$ and represents an empirical "buildup" factor, while μ is the effective "buildup" relaxation length and λ is an effective interaction length. Nearly all of existing measurements are well described by taking μ to be 56 meters. Q is the source strength that dimensionally must be consistent with $\Phi(r)$. Thus, for the standard meaning of $\Phi(r)$ as the fluence, Q is the number of neutrons emitted by the source. A plot of this function for a variety of choices of the value of λ is given in Fig. 4.11. Values of $\lambda > 830$ meters are possible if very high energy neutrons ($E > 150$ MeV) are present. Such large values of λ are more likely due to multiple sources or an extended source. In such circumstances, the radiation field may also not necessarily be isotropic. A value of 830 m (100 g/cm² of air at standard temperature and pressure) corresponds to the interaction of the neutrons of approximately 100 MeV likely to control the propagation of hadronic cascades in air. Thus, λ is determined by the neutron energy spectrum present at the

Chapter 4 Low Energy Prompt Radiation Phenomena

thinly shielded location. Cossairt and Coulson (Co85b) present an example of a non-isotropic, complex skyshine source involving high energies and an extremely thin shield which resulted in a value of $\lambda \approx 1200$ meters.

The procedure, then, for using Eq. (4.15) is to:

- A. Estimate the total emission rate of neutrons from the source. This can be done by using information about the neutron spectrum at the source to choose an "average" energy and intensity. The flux density to dose equivalent rate factor at that energy can then be used in conjunction with a dose equivalent rate survey over the thinly shielded region to determine the total neutron emission rate, Q , by numerically integrating over the area of the top of the shield.
- B. Estimate the value of λ from the neutron energy spectrum information.
- C. Apply Eq. (4.15) to determine the radial dependence.

A somewhat more rigorous treatment has been reported by Stevenson and Thomas (St84) which utilized the work of Nakamura and Kosako (Na81) and of Alsmiller, Barish, and Childs (Al81). Stevenson and Thomas parameterized the phenomena with the following equation:

$$\Phi(r) = \frac{Q'}{4\pi r^2} e^{-r/\lambda}. \quad (4.16)$$

In this equation, the buildup exponential factor has been suppressed so the formula is valid only at large distances (i.e., $r \gg 56$ meters). In addition, the quantity denoted by Q' implicitly includes the buildup factor of 2.8.

Alsmiller and Nakamura have separately performed extensive Monte-Carlo calculations of the neutrons emitted into cones of small vertex angle. Nakamura and Kosako used the Monte-Carlo code MORSE while Alsmiller, Barish, and Childs used the Discrete Ordinates Transport Code DOT. For selected distances from the skyshine source, these workers have calculated the dose equivalent as a function of both the source neutron energy and the emission cone's semivertical angle (that is, the half-angle the rotation of which defines the cone into which the neutrons are emitted). The authors define this quantity, the so-called **neutron importance**, as the dose equivalent at a distant location as a function of the energy of the emitted neutron. The terminology is this a calculation of how "important" a given emitted neutron is in delivering ionizing radiation to location at a given distance. The results of the Alsmiller calculation for small semivertical angles are given in Fig. 4.12. The corresponding, but somewhat less-detailed results of Nakamura, are in good agreement with these results.

Stevenson and Thomas (St84) were able to derive an alternative "recipe" for skyshine neutron calculations by making two assumptions:

Chapter 4 Low Energy Prompt Radiation Phenomena

- A. The neutron spectrum has the $1/E$ form up to the proton energy and zero at higher energies. This likely overestimates the contribution of the higher energy neutrons.
- B. The neutrons are emitted into a cone whose semivertical angle is about 70-80°. This may overestimate the doses by up to a factor of three for sources of smaller semivertical angles.

Further, they used the Alsimiller importance functions to estimate the value of λ based upon the upper energy of the $1/E$ spectrum. Fig. 4.13 displays the results of doing this for several choices of upper energies at three distances in a plot in which the $1/r^2$ dependence is suppressed. The slopes, then, were used to obtain values of λ as a function of "upper energy" which are plotted in Fig. 4.14. A comparison with a measurement conducted at Brookhaven National Laboratory is also provided. To determine the source term, the straight lines in Fig. 4.13 (on the semi-logarithmic plot) were extrapolated to zero and used to determine intercepts at $r = 0$ ranging from 1.5×10^{-15} to 3×10^{-15} Sv $m^2/\text{neutron}$ (1.5×10^{-13} to 3×10^{-13} rem $m^2/\text{neutron}$). Hence, conservatively, Stevenson and Thomas found that

$$H(r) = \frac{3 \times 10^{-13}}{r^2} e^{-r/\lambda} \quad (\text{rem/neutron, } r \text{ in meters}). \quad (4.17)$$

Again, one has to determine the total number of neutrons emitted. This can be done as before by measuring the integral of dose equivalent times the area over the thinly shielded location and using the reciprocal of the dose equivalent/fluence conversion factor to get the total number of neutrons emitted. The use of the above formula will lead to an overestimate of neutrons for values of r less than approximately 100 meters because the extrapolation ignores the observed exponential buildup of the skyshine.

Stevenson and Thomas (St84) give a convenient table of dose-equivalent per fluence conversion factors derived from data in ICRP Publication 21 (IC73) integrated over such $1/E$ spectra which is provided here as Table 4.4.

Measurements at Fermilab (Co85b) have confirmed this general method for a "source" involving the targetry of 400 GeV protons. Figure 4.15 from this work shows two measured and fitted radial distributions made using Eq. (4.15). In Fig. 4.15, "Survey 2" corresponds to a shielding configuration where the neutron energy spectrum was inferred to be of very high energy while "Survey 4" was likely to involve a softer spectrum. Survey 4 was made for the same beam and target after the concrete shield thickness around the source was greatly increased compared with the shield present when "Survey 2" was obtained. The normalization to "counts- m^2/hr " refers to an integration of an instrumental response over the surface area of the source and should be approximately proportional to the emitted neutron fluence. The instrument calibration of "counts/hr" made possible an estimate of dose rates at $r = 200$ meters for the two surveys. One can make an educated guess that the conditions of "Survey 2" correspond to an upper energy of 1 GeV, while the conditions of "Survey 4" correspond to an approximate upper energy of 100 MeV.

Chapter 4 Low Energy Prompt Radiation Phenomena

Using the appropriate dose equivalent/fluence, the value of Q for the Survey 2 conditions was determined experimentally to be 2.5×10^5 mrem m^2/hr . This was obtained from the measured absorbed dose surface integral of 5×10^4 mrad m^2/hr and assuming a quality factor of 5. For the Survey 4 conditions, Q was found to be 4.0×10^4 mrem m^2/hr . Again, this was obtained from the measured absorbed dose surface integral of 8.1×10^3 mrad m^2/hr and assumed a quality factor of 5. Table 4.5 makes a comparison with the prescription of (St84) for these data. In this table, H is the dose equivalent in one hour at 200 meters. The prescription of Stevenson and Thomas (St84) is used to calculate the dose equivalent in one hour at 200 meters. The agreement is well within all uncertainties involved.

A final illustration is provided by Elwyn and Cossairt (El86) who described the thin iron shield addressed by Figs. 3.21. Fig. 4.16 taken from (El86) shows the radial dependence of neutron flux. In this measurement, λ was determined to be 184.4 m by fitting this radial dependence using Eq. (4.15). The "source" is that shown in Fig. 3.21 and described in Chapter 3. It is thus known that the neutron radiation field is dominated by neutrons of energies near 847 keV insofar as skyshine is concerned. One can use the parametrization of Elwyn and Cossairt to reproduce the measured fluence, normalized to 10^{12} incident protons, at, say, $r = 200$ meters using Eq. (4.15), where parameters $Q = 1.75 \times 10^{10}$ and $\lambda = 184.4$ meters were determined by fitting the skyshine data:

$$\Phi(200) = \frac{2.8(1.75 \times 10^{10})}{4\pi (200)^2} [1 - \exp(200/56)] \exp(-200/184.4) = 3.20 \times 10^4 \text{ neutrons } m^{-2}. \quad (4.18)$$

Thus, taking the measured neutron flux at $r = 200$ meters and applying an appropriate dose equivalent/fluence value gives a dose equivalent per 10^{12} incident protons of 8.7×10^{-5} mrem at $r = 200$ meters. The value of λ which fitted the skyshine data is also consistent with the neutron energy spectrum, which was known to be dominated by neutrons of less than 1 MeV kinetic energy.

Elwyn and Cossairt also estimated the total neutron emission of the source to be $(3.4 \pm 2.0) \times 10^{10}$ per 10^{12} incident protons by performing a numerical integration over the surface area of the source separate from the result determined using the skyshine measurement. Applying the prescription of Stevenson and Thomas (St84) found in Eq. (4.14):

$$\begin{aligned} H(200) &= \frac{(3 \times 10^{-13})[(3.4 \pm 2.0) \times 10^{10}]}{(200)^2} \exp(-200/184.4) = \\ &= (8.6 \pm 5.1) \times 10^{-5} \text{ mrem at this same location.} \end{aligned} \quad (4.19)$$

Thus the consistency of the two methods is verified.

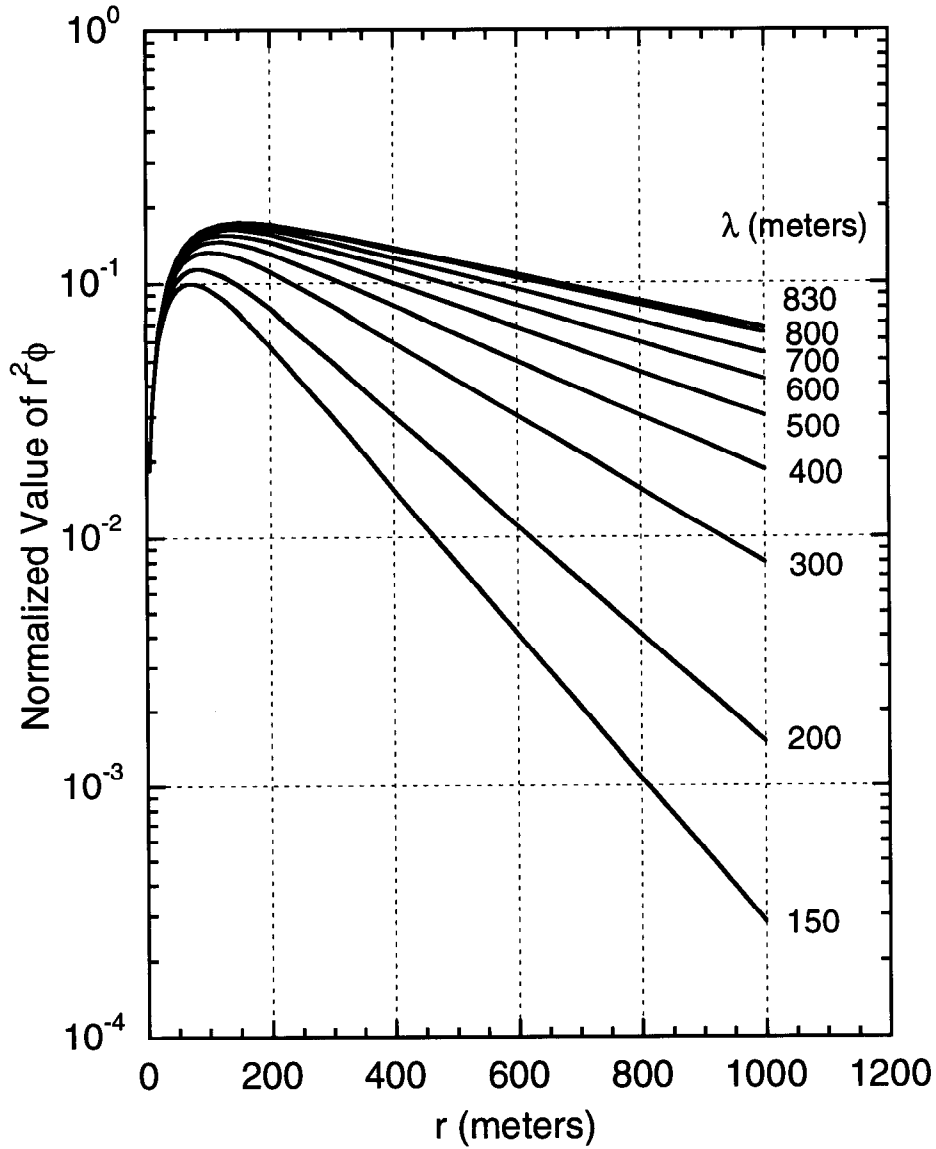


Fig. 4.11 Plot of skyshine distributions according to Eq. (4.15) for a variety of values of λ . The ordinate is the quantity $r^2\phi(r)$ in that equation for a value of $Q = 1$.

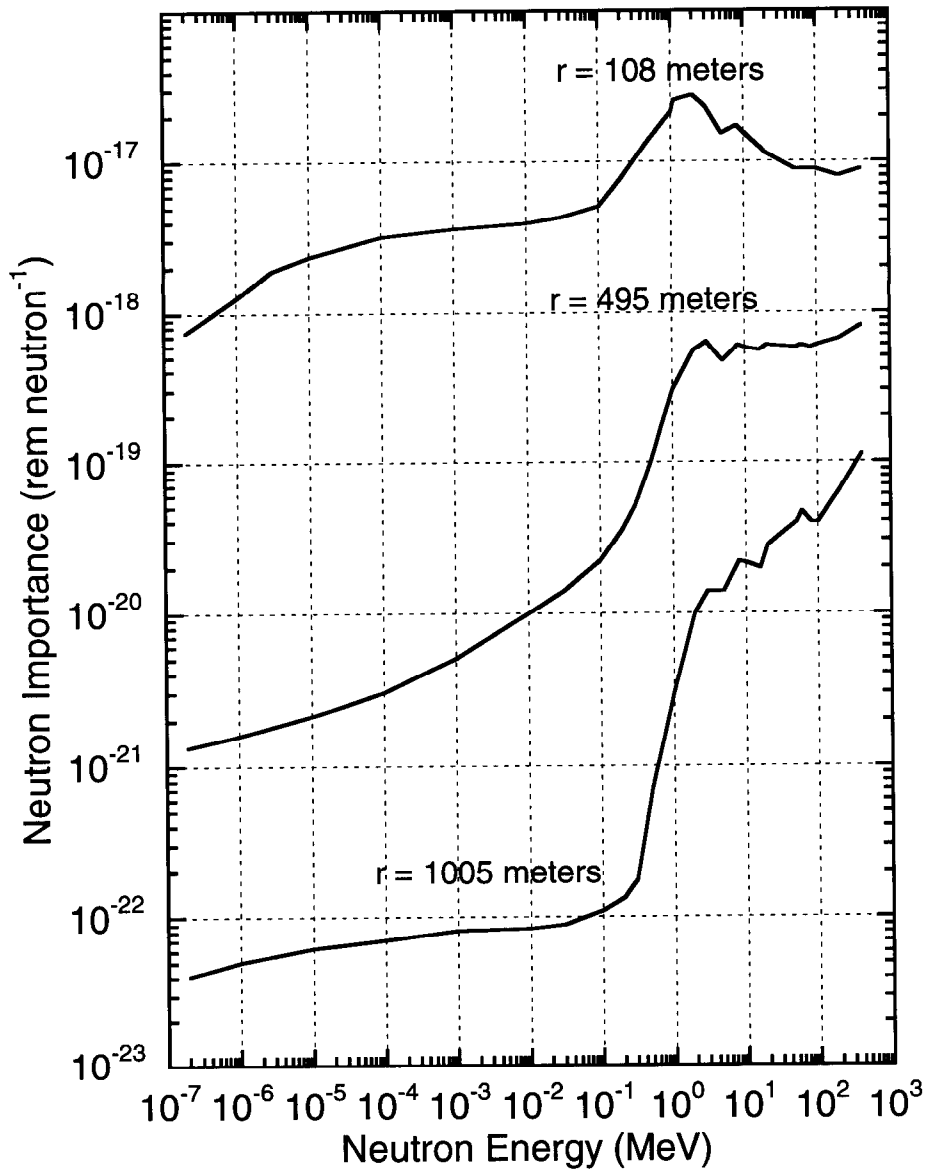


Fig. 4.12 Neutron skyshine importance functions for small semivertical cone angles at three different values of the distance from a point source. The curves are those of Alsmiller et al. (A181).

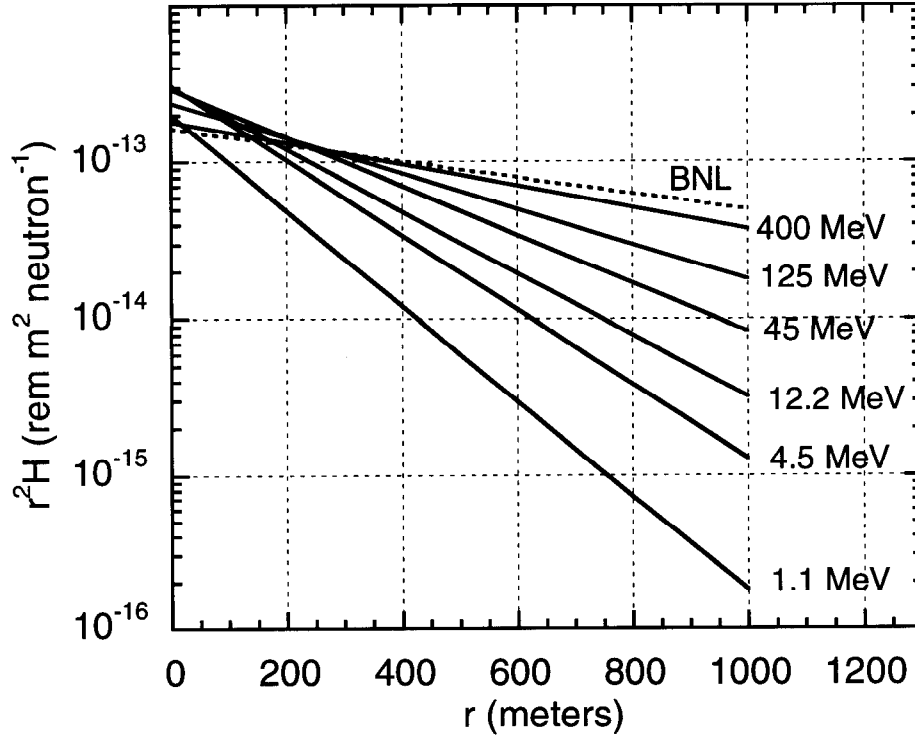


Fig. 4.13 Variation of does equivalent with distance r for $1/E$ neutron spectra with different upper energies. The ordinate is dose equivalent H times distance squared. The curve labeled "BNL" is a measurement. [Adapted from (Sc90).]

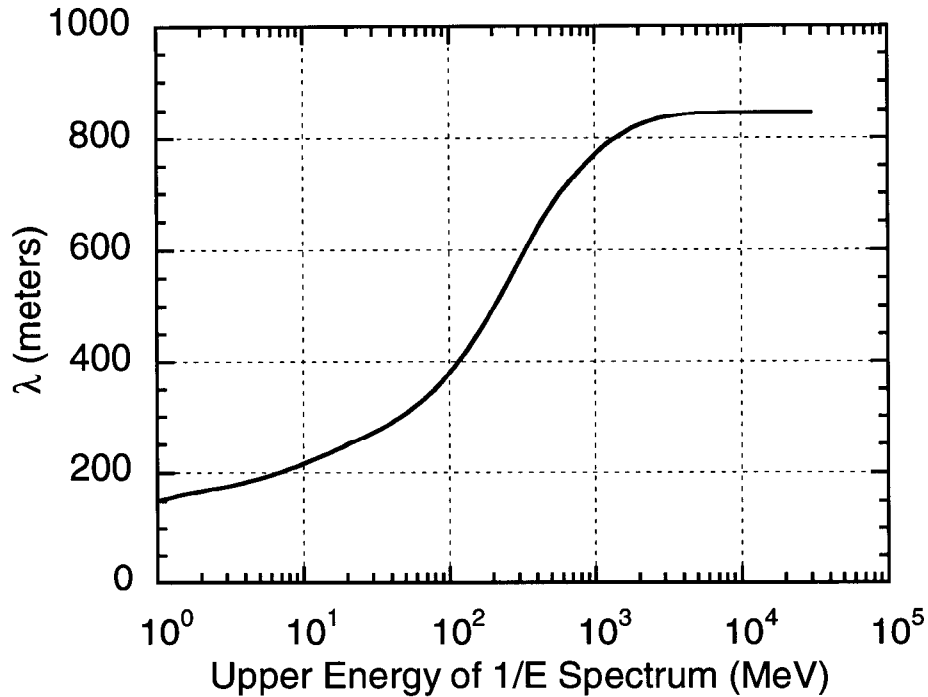


Fig. 4.14 Effective absorption length λ as a function of upper neutron energy E for $1/E$ spectra. [Adapted from (Sc90).]

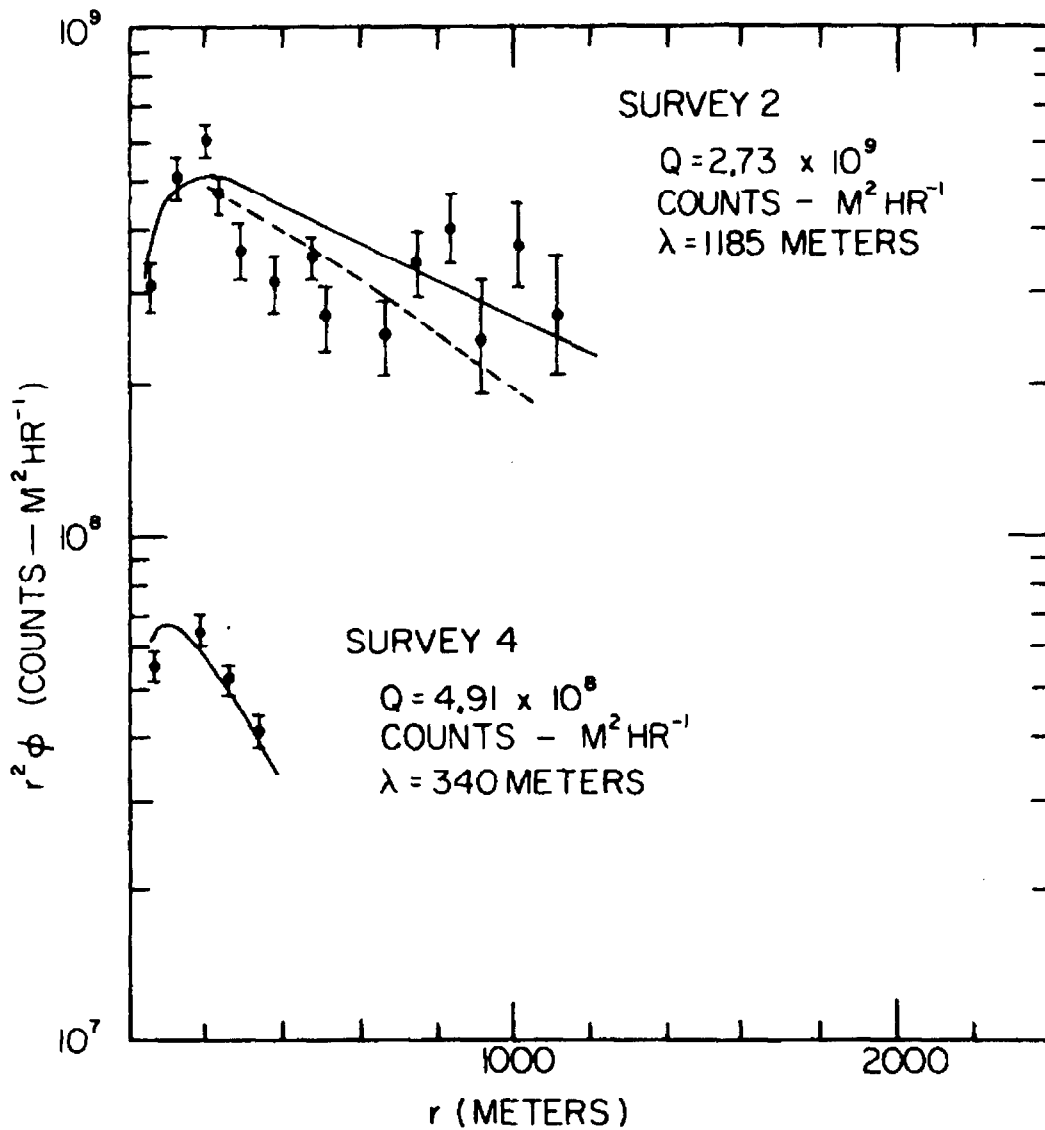


Fig. 4.15 Skyshine data from two different surveys plotted as $r^2\phi$ as a function of distance from the source r . The solid curves are from the least squares fit of Eq. (4.15) to the data points while the dashed curve is the fit if λ is constrained to have a value of 830 m. Error bars represent 1 standard deviation counting statistics. [Reproduced from (Co85b).]

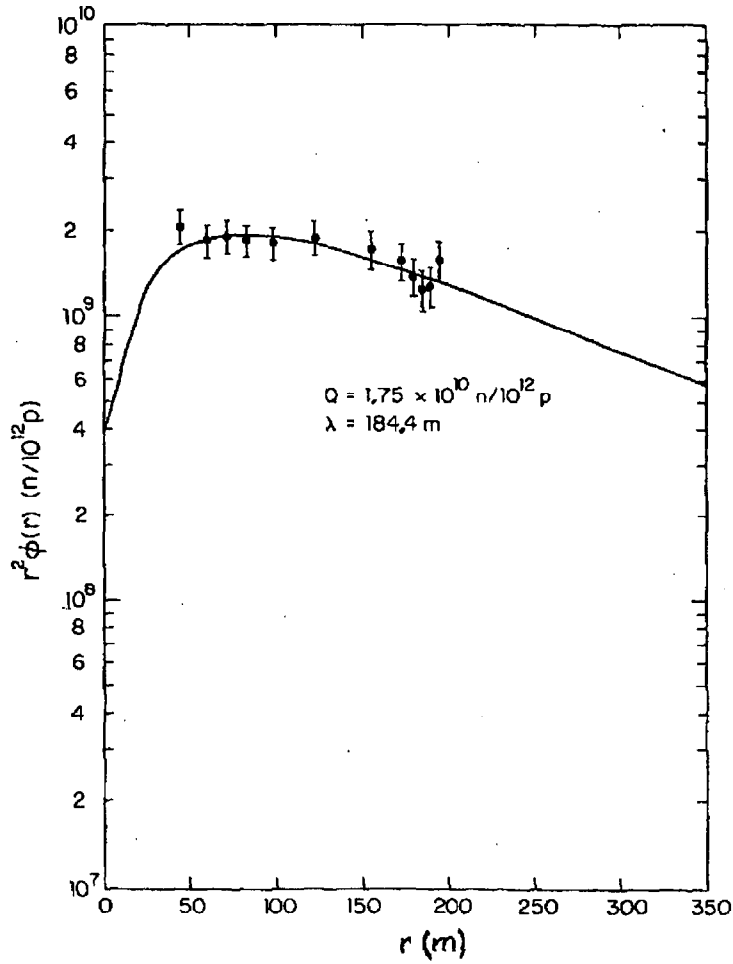


Fig. 4.16 The product of r^2 and the neutron fluence $\phi(r)$ per 10^{12} protons incident on a target as a function of the distance from the source r . The source is that described in connection with Fig. 3.21. The smooth curve is a fit to Eq. (4.15) with parameters $\lambda = 184.4 \text{ m}$ and $Q = 1.74 \times 10^{10}$ neutrons per 10^{12} protons. [Reproduced from (E186).]

Chapter 4 Low Energy Prompt Radiation Phenomena

Table 4.4 Dose equivalent per neutron/cm² for 1/E Neutron Spectra of Different Upper Energies [Adapted from (St84).]

Upper Energy (MeV)	Spectrum Averaged Dose Equivalent Conversion (10 ⁻⁹ rem/(n cm ⁻²))
1.6	3.9
2.5	4.8
4.0	5.6
6.3	6.4
10	7.2
16	7.9
25	8.6
40	9.4
63	10.1
100	10.9
160	11.7
250	12.5
400	13.4
630	14.6
1000	16.2
1600	18.4
2500	21.2
4000	25.0
6300	30.0
10000	36.5

Table 4.5 Comparisons of Fermilab skyshine data with results of parameterizations of surveys shown in Fig. 4.15, assuming 1/E spectra with inferred upper energies. The quantities are all for a one hour time period.

Survey	λ (meters) (Co85b)	E_{\max} (inferred) (MeV)	Dose Equiv per Fluence (mrem/ n cm ⁻²) (St84)	Q - measured (mrem m ²) (Co85b)	H (200 m) (mrem)- calculated	H (200 m) (mrem)- measured (Co85b)
Survey 2	1200	1000	16.2×10^{-6}	2.5×10^5	1.0	1.6
Survey 4	340	100	10.9×10^{-6}	4.0×10^4	0.15	0.15

Chapter 4 Low Energy Prompt Radiation Phenomena

References

- (Al81) R. G. Alsmiller, J. Barish, and R. L. Childs, "Skyshine at neutron energies < 400 MeV", Part. Accel. 11 (1981) 131-141.
- (Ch63) A. B. Chilton and C. M. Huddleston, "A semi-empirical formula for differential dose albedo for gamma rays on concrete", Nucl. Sci. Eng. 17 (1963)419.
- (Ch64) A. B. Chilton, "Backscatter for gamma rays from a point source near a concrete plane surface", Univ. Illinois Eng. Sta. Bull. No 471 (University of Illinois, Urbana, Illinois, 1964).
- (Ch65a) A. B. Chilton, "Backscattering of gamma rays from point sources by an infinite-plane concrete surface", Nucl. Sci. Eng. 21 (1965) 194-200.
- (Ch65b) A. B. Chilton, C. M. Davisson, and L. A. and Beach (1965). "Parameters for C-H albedo formula for gamma rays reflected from water, concrete, iron, and lead", Trans. Am. Nucl. Soc. 8, No. 2, (1965) 656.
- (Co73) M. O. Cohen, W. Guber, E. S. Troubezko, H. Lichtenstein, and H. A. Steinberg, "SAM-CE, a three dimensional Monte-Carlo code for the solution of the forward neutron and forward and adjoint gamma ray transport equations", Rept. DNA-2830-F, Rev. B Defense Nuclear Agency, Washington, DC (1973).
- (Co85a) J. D. Cossairt, J. G. Couch, A. J. Elwyn, and W. S. Freeman, "Radiation measurements in a labyrinth penetration at a high-energy proton accelerator", Health Phys. 49 (1985) 907-917.
- (Co85b) J. D. Cossairt and L. V. Coulson, "Neutron skyshine measurements at Fermilab", Health Physics 48 (1985) 171-181.
- (Co95) J. D. Cossairt, "Approximate technique for estimating labyrinth attenuation of accelerator-produced neutrons", Fermilab Radiation Physics Note #188, October 1995.
- (D'H68) M. M. D'Hombres, C. Devillers, F. Gervaise, B. De Sereville, and P. Tardy-Joubert, "Propagation des neutrons dans les tunnes d'Accès à un accélérateur de haute energie à protons", Rep. CEA-R-3491, Centre d'études nucléaires de Saclay (1968).
- (El86) A. J. Elwyn and J. D. Cossairt, "A study of neutron leakage through an Fe shield at an accelerator", Health Physics 51 (1986) 723-735.

Chapter 4 Low Energy Prompt Radiation Phenomena

- (El91) A. J. Elwyn to J. D. Cossairt, private communication (1991).
- (Gi69) W. S. Gilbert, "Shielding measurements at the CERN 25 GeV proton synchrotron", Rept. CONF-691101, USAEC 323 (1969)
- (Go71) P. J. Gollon and M. Awschalom, "Design of penetrations in hadron shields", CERN Report 71-16 Vol. 2 (1971) also published in IEEE Trans. Nucl. Sci NS-18 (1971)741-745.
- (Go75) K. Goebel, G. R. Stevenson, J. T. Routti, and H. G. Vogt, "Evaluating dose rates due to neutron leakage through the access tunnels of the SPS", CERN Report. LABII-RA/Note/75-10 (1975).
- (IC73) International Commission on Radiological Protection, "Data for protection against ionizing radiation from external sources, supplement to ICRP Publication 15", ICRP Publication 21 (Oxford, Pergamon Press, 1973).
- (Li61) S. J. Lindenbaum, "Shielding of high energy accelerators", Ann. Rev. Nucl. Sci. 11 (1961) 213-258.
- (Ma67) R. E. Maerker and V. R. Cain, "AMC, a Monte-Carlo code utilizing the albedo approach for calculating neutron and capture gamma-ray distributions in rectangular concrete ducts", Rep. ORNL-3964, Oak Ridge National Laboratory, Oak Ridge, Tennessee (1967).
- (Na81) T. Nakamura and T. Kosako, "A systematic study on neutron skyshine from nuclear facilities, Part I: Monte-Carlo analysis of neutron propagation in air-over-ground environment from a monoenergetic source", Nucl. Sci, and Eng. 77 (1981) 168-181.
- (NC77) E. A. Burrill, Chair, J. R. Beyster, G. L. Brownell, A. B. Chilton, J. Haimson, C. J. Karzmark, W. E. Kreger, J. M. Wyckoff, *Radiation protection design guidelines for 0.1-100 MeV particle accelerator Facilities*, National Council on Radiation Protection and Measurements, NCRP Report 51 (1977).
- (Pa73) H. W. Patterson and R. H. Thomas, *Accelerator health physics*, Academic Press, New York, 1973.
- (Ra91) R. Rameika, "Labyrinths and penetration methodology-Version 1.3", Fermilab Research Division Shielding Assessment (1991), private communication (1991).
- (Ri75) A. Rindi and R. H. Thomas, "Skyshine-a paper tiger?", Particle Accelerators 7 (1975) 23-39.

Chapter 4 Low Energy Prompt Radiation Phenomena

- (Ru76) P. Ruffin and C. Moore, "A study of neutron attenuation in the E-99 labyrinth", Fermilab Radiation Physics Note # 9 (1976).
- (Sc90) H. Schopper (editor), A. Fassò, K. Goebel, M. Höfert, J. Ranft, and G. Stevenson, *Landolt-Börnstein Numerical data and functional relationships in science and technology new series; group I: nuclear and particle physics Volume II: shielding against high energy radiation* (O. Madelung, Editor in Chief, Springer-Verlag, Berlin, Heidelberg, 1990).
- (St73) G. R. Stevenson and D. M. Squier, "An experimental study of the attenuation of radiation in tunnels penetrating the shield of an extracted beam of the 7 GeV proton synchrotron NIMROD, Health Physics 24 (1973) 87-93.
- (St84) G. R. Stevenson and R. H. Thomas, "A simple procedure for the estimation of neutron skyshine from proton accelerators", Health Physics 46 (1984) 115-122.
- (Te82) K. Tesch, "The attenuation of the neutron dose equivalent in a labyrinth through an accelerator shield", Particle Accelerators 12 (1982) 169-175.
- (Th88) R. H. Thomas and G. R. Stevenson, "Radiological safety aspects of the operation of proton accelerators", Technical Report No. 283, International Atomic Energy Agency, Vienna, 1988.

Chapter 4 Low Energy Prompt Radiation Phenomena

Problems

1. A $1 \mu\text{A}$ 100 MeV electron beam is incident on an "optimized bremsstrahlung" target in a shielding configuration and labyrinth like that in Fig. 4.3. Using the facts given in Chapter 1 (Swanson's Rules of Thumb, etc.) about bremsstrahlung, calculate the dose equivalent rate at the exit of a labyrinth having 2 legs. Set all distances, d_i , d_1 , and $d_2 = 3$ meters. If the goal is to get the dose equivalent rate at the exit to be < 1 mrem/hr, is this a sensible design? The 2 legs are 1×2 meter² in cross section and, since no other information is available, use $\alpha = 10^{-2}$ as a "conservative" value. [Hint: One needs to calculate the projected diameter of the beam at the wall where the first scatter occurs. This can be done using Eq. (1.28).]
2. A 500 GeV proton beam of 10^{11} protons/second strikes a magnet 2 m from the mouth of a 3-legged labyrinth. Each of the 3 legs is 4 meters long and 1×2 m² in cross section. Assume the source is an on-axis "point source". Using Goebel's "universal" curves and Rameika's source term, what is the dose equivalent rate at the exit expressed in rem/hr. How far away from the exit does the value of dH/dt fall to 10 mrem/hr.
3. A high energy accelerator has a section of beamline which was poorly designed. Beam losses and insufficient shielding have resulted in a region of roof 10 meters wide and 50 meters long where a neutron dose equivalent rate averaging 100 mrem/hour (averaged over the surface of the weak shield) is found. A spectrum measurement indicates the spectrum to be approximately $1/E$ with an upper end point of approximately 500 MeV. Calculate the dose equivalent rate due to skyshine at distance $r = 50, 100, 200, 500, \& 1000$ m using both formulae presented here.

